International Journal of Fracture **80:** 165–192, 1996.

Recent advances in fatigue crack growth modeling

HUSEYIN SEHITOGLU, K. GALL and A.M. GARCÍA
Department of Mechanical and Industrial Engineering, University of Illinois at Urbana-Champaign, Urbana, Il. 61801, USA

Received 16 January 1996; accepted in revised form 30 July 1996

Abstract. Recent advances in our understanding of fatigue crack growth processes and respective crack growth modeling techniques are reviewed. Much of the observed experimental behavior (such as the effects of notches, maximum applied stress, crack length, in-plane biaxiality, out-of-plane constraint, and transient loadings) can be explained based on crack closure concepts. Both Dugdale based models and finite element techniques have been utilized. However, so far neither approach has accounted for crystallographic slip effects, grain orientation effects, or microstructural barriers. A model for crack closure with two microscopic crystallographic slip directions is used to model microscopic cracks. The model predicts variations in closure levels as the orientations of the two slip directions, with respect to the crack growth direction, are changed. In addition, a solution is proposed for the asperity micro-contact problem through a unique roughness induced closure model using a statistical description of asperity heights, asperity densities, and material flow properties.

Nomenclature

A, B, D = Constants in $S_{\text{open}}/S_{\max}$ equation for crack growth from a notch
a = Crack length including half notch width $a = 1 + c$, also crack length in CT specimen
b = Half notch depth
c = Half notch width
c' = Constant relating back stress to shear strain on slip system α
C' = Material constant in crack growth equation
C = Nondimensional measure of asperity deformation
CCT = Center cracked tension specimen
CT = Compact tension specimen
d_i = Crack opening displacement of strip i
$\mathrm{d}a/\mathrm{d}N$ = Crack growth rate
$\mathrm{d}\overline{\varepsilon^p}$ = Equivalent plastic strain increment
$\mathrm{d}\overline{\sigma}$ = Equivalent stress increment
E = Elastic modulus
ε_0^p = Constant in power law stress strain relationship
$\dot{\varepsilon}_c^0$ = Creep constant
$\varepsilon_x^p, \varepsilon_z^p$ = Plastic strains in x and z directions at crack tip at minimum load
$\gamma^{(\alpha)}$ = Shear strain on slip system α
F = Crack length dependence in $S_{\text{open}}/S_{\max}$ equation
F.E.M. = Finite element model
G = Material constant for power law hardening
H = Hardening modulus
J_2 = Second invariant of deviatoric stress
$K_{\max}$ = Maximum stress intensity

ΔK = Stress intensity range
ΔK_{eff} = Effective stress intensity range
K_t = Theoretical elastic stress concentration factor
k = Yield stress in shear
l = Crack length measured from notch root (CCT specimen)
$\lambda^{(\alpha)}$ = Resolved shear stress on slip system α
λ_0 = Critical resolved shear stress
λ = S_x/S_y (transverse to normal stress ratio)
m = Creep exponent
m' = Exponent crack growth equation
m_1, m_2 = Unit vectors characterizing the slip plane normal
n = Number of asperities
N = Material constant of power law hardening
ϕ = The orientation of the crystal
P = Normal traction between two asperities
$P_{\max}$ = Maximum applied load level
$P_{\min}$ = Minimum applied load level
P_0 = Limit load for CT specimen
P_{open} = Crack opening load level at which the residual stresses on the crack faces are relieved
p_0^s = Contact pressure corresponding to shakedown conditions in contact
P_t = Applied tensile load level at which all stresses in the uncracked ligament become tensile
P_{tt} = Applied tensile load level at which stresses immediately ahead of crack tip become tensile
Q = Shear traction between two asperities
R_i' = Radius of the tip of asperity i
R = Applied load ratio
R' = Average radius of asperity tips
R-ICC = Roughness induced crack closure
ρ = r.m.s. of asperity heights
r_p = Notch plastic zone size
S_{ij} = Deviatoric stress
s_1, s_2 = Unit vectors characterizing the slip plane direction
$S_{\max}$ = Maximum applied stress level
$S_{\min}$ = Minimum applied stress level
S_{open} = Crack opening stress level at which the residual stresses behind crack tip are overcome
$S_{\text{open}}^{\text{stable}}$ = Stabilized crack opening stresses for crack growing from a notch
S_t = Applied tensile stress level at which all stresses in the uncracked ligament become tensile
S_{tt} = Applied tensile stress level at which stresses immediately ahead of crack tip become tensile
S_x = Applied stress transverse (parallel) to crack
S_y = Applied stress normal to crack
$\overline{\sigma}$ = Von Mises equivalent stress
σ_H = Hydrostatic stress
σ_0 = Uniaxial yield strength
$\sigma_c^{(\alpha)}$ = Back stress on the slip plane α
σ_c = Creep constant
Θ = The half plane between the two slip planes
t_h = Hold period at maximum stress
U = Effective stress ratio
U_0 = Effective stress ratio when hold period is zero
x, y, z = Coordinate axis (x-crack growth direction, z = thickness direction)
z_i = height of asperity

1. Introduction

There have been numerous research studies on the characterization of fatigue crack growth using fracture mechanics since the work of Paris and colleagues [1] in the early 1960's. Following this work, in the early 1970's, Elber [2–3] pioneered the concept of premature crack closure and it's relation to fatigue crack advance. In the late 1970's and mid 1980's many researchers [4–41] then incorporated fatigue crack closure concepts into descriptions of crack growth. These descriptions rely on the effective stress intensity range as the driving force for fatigue crack growth rates. As the attention turned to 'advanced' materials in the late-80's there has been less emphasis on advancing the understanding of crack closure concepts, and crack advance mechanisms in fatigue. It is probably in the last two years that the topic has received renewed attention [42–45].

The universal description of crack growth rates is given by

$$\frac{da}{dN} = C'(\Delta K_{\text{eff}})^{m'}. \tag{1}$$

In (1) C' and m' are material constants, and ΔK_{eff} is the effective stress intensity range which is a function of several variables:

$$\Delta K_{\text{eff}} = f\left(\frac{S_{\max}}{\sigma_0}, R, \frac{H}{E}, \frac{\overline{\sigma}}{\sigma_H}, \text{ Geometry, Microstructure, } a\right). \tag{2}$$

Early models for the effective stress intensity range considered only the R-ratio effect primarily at positive R ratios [2–3]. Then, the effect of other factors such as the applied stress, $S_{\max}/\sigma_0$, were studied [9, 21–23, 28]. The effect of $S_{\max}/\sigma_0$ is observed through constant amplitude testing at different maximum stress (or load) levels. The $S_{\max}/\sigma_0$ effect is caused by crack tip geometry changes, deviations from small scale yielding, and decreases in the elastic constraint. Increasing $S_{\max}/\sigma_0$ modifies the crack opening displacement profiles, which in turn lowers the crack closure levels. A variation in $S_{\max}/\sigma_0$ during the loading history creates a history effect. In the presence of a variable amplitude history, including overloads or high-low sequences the crack closure levels behave differently than under constant amplitude loading.

The H/E (plastic modulus/elastic modulus) ratio or the strain hardening exponent also have an effect on crack closure levels. In the Dugdale models [8–9] this effect has been rationalized by altering the value of σ_0. Using finite elements [21–23] it has been possible to change H/E (or the strain hardening exponent) independent of σ_0. As the $S_{\max}/\sigma_0$ level increases, the lower hardening materials exhibit the lowest opening levels. At low $S_{\max}/\sigma_0$ levels the trends are reversed.

The $\overline{\sigma}/\sigma_H$ parameter represents the ratio of effective stress to hydrostatic stress ratio and is a measure of the stress state or constraint on the cracked member. Several modeling efforts have focused on plane stress versus plane strain (termed out-of-plane constraint) conditions [30, 35, 41] and in plane constraint [48, 49] where the stresses are applied both perpendicular and parallel to the crack. In general as $\overline{\sigma}/\sigma_H$ increases the closure levels decrease.

The specimen geometry and crack length have an influence on crack growth rates. The crack growth rates of cracks growing from notches are higher than expected when using the same ΔK or ΔJ as for long fatigue cracks. There are some differences in the crack growth rates of the compact tension specimen (CT) and the center cracked tension specimen (CCT) since the stress intensity factor is often higher for the CT specimen at the same $S_{\max}/\sigma_0$ ratio. The inplane stresses are also slightly different from specimen to specimen which also affect

the results. The crack length also has an influence on closure levels. Even in the absence of microstructure effects, small cracks do not have a sufficient wake to develop closure. As the crack grows the wake develops and steady state closure conditions are reached.

The microstructure has a considerable influence on crack closure, particularly near the threshold stress intensity regime. One of the shortcomings of the existing models is that they treat material ahead of crack tips as an isotropic continuum. It is well known that plastic deformation ahead of crack tips is confined to specific slip systems and the use of crystal plasticity concepts would be more appropriate for fatigue analysis. This will be considered in the paper. The other limitation of the ΔK_{eff} models is that the crack path develops a roughness depending on the grain orientation, periodic barriers, and slip character. The current roughness induced closure models are too idealistic to handle the microcontact phenomena which include sliding displacements that develop as the crack advances. However, a model has recently been developed which addresses all of these issues [45].

Numerous papers have been published by Sehitoglu and his colleagues on fatigue crack closure to explain a variety of effects on fatigue crack growth. We will provide an account of our research on maximum stress level effects [22–23, 28], notch effects [6, 16, 21, 24], variable amplitude loading effects [7], the role of tensile stresses ahead of a crack tip [30, 35, 41], microstructure effects (microscopic plasticity and roughness induced closure [42–47]), in-plane and out-of-plane constraint [35, 40, 41, 48–49], and time dependent crack growth effects [50].

More explicitly, the purpose of the present work is:

(i) to discuss plasticity induced fatigue crack closure as a function of $S_{\max}/\sigma_0, R, H/E, \overline{\sigma}/\sigma_H$, geometry, and hold period, then compare experimental results and models
(ii) to study the effect of microstructure on closure using a crystal plasticity double slip model modified for cyclic loading
(iii) to model roughness induced crack closure using contact mechanics concepts.

2. Approach

A specialized two dimensional elastic-plastic finite element code with provision for cyclic crack growth was used for part of this study. The code was initially generated by Lalor and Sehitoglu [6, 21], modified by McClung and Sehitoglu [22–23] and further modified by Kadioglu, Sehitoglu, and Gall [42–44].

The isotropic and homogeneous material model was developed using the concepts of incremental rate independent plasticity. A Von Mises yield criteria with kinematic hardening was employed to capture the Bauschinger effect during cyclic loading. The hardening modulus, $H = \mathrm{d}\overline{\sigma}/\mathrm{d}\overline{\varepsilon^p}$, was chosen as a constant equal to 0.001E or 0.07E. To simulate nonlinear hardening the plastic modulus was written as a function of stresses $H = (GJ_2^N)$ where $J_2 = 1/2S_{ij}S_{ij}, S_{ij}$ is the stress deviator, and G and N are material constants.

Two different cracked geometry's were studied, the center cracked tension (CCT) specimen and the compact tension (CT) specimen (Figure 1). Both circular and elliptical notches were considered for the CCT specimen. Four noded isoparametric elements with linear strain distributions were used for the model since higher order elements greatly increase the computation time in cyclic loading models. In the CT specimen, the plastic zone ahead of the crack tip is very small compared to the crack length and the width of the specimen. However, the plastic zone can be fairly large compared with the crack length and CCT specimen width,

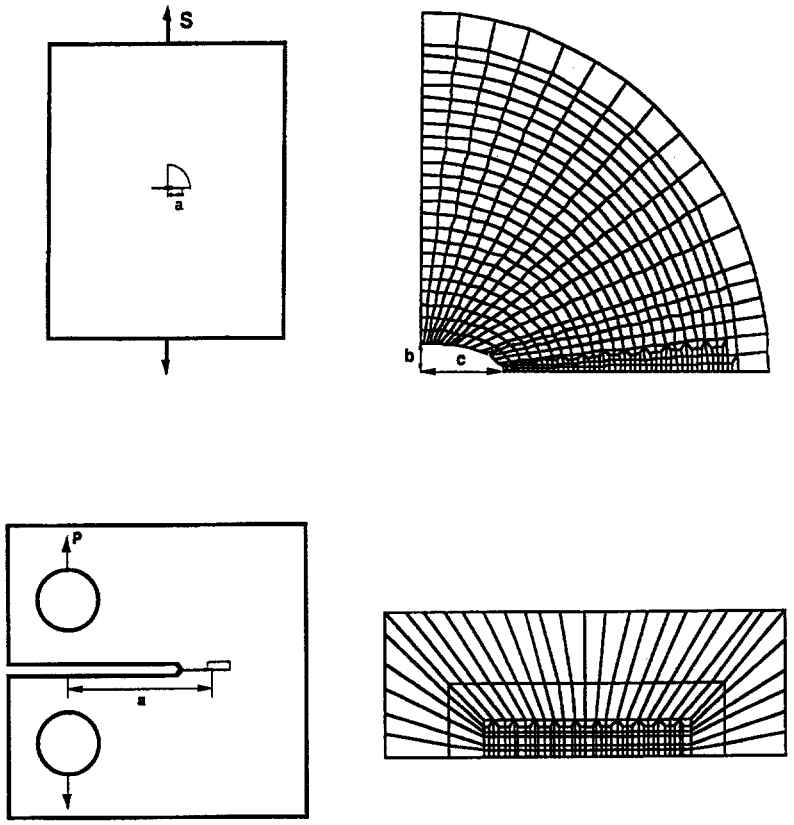

Figure 1. Specimen geometry's used in fatigue crack closure research.

and may reach the edge of the specimen when a high stress is applied. Therefore, the results from a CCT specimen are considered as outside the small scale yielding regime. Most of the computational details of the two dimensional model have been previously released [21–23]. The term P_{max}/P_0 will be used for the CT specimen where P_{max} is the maximum load and P_0 is the limit load [35, 41]. The term S_{max}/σ_0 will be used for the CCT specimen where S_{max} is the maximum stress and σ_0 is the yield stress [35, 41].

Twenty to thirty loading cycles were applied to the specimen so that the crack opening stresses could reach stabilized values. A crack tip node is released at the first increment of the unloading reversal, creating an effective crack growth increment of one fine mesh unit per cycle. Previous study [22] has shown that there is no significant effect of the node release scheme on crack opening stress levels. In the numerical model, it is not possible to choose crack increments comparable to experimental crack growth rate per cycle, as this would result in enormous computation times. The size of the crack increments, though, is not likely to change the closure levels provided that the model is fine enough to capture the plastic deformation near the crack tip. The finite element model permits study of both stationary cracks and fatigue cracks. To obtain a fatigue crack, one crack tip node was released and the crack was advanced at maximum load on each loading cycle. The stationary crack had no nodal release scheme, hence no crack remained in the same position throughout the simulation. In this study, the crack opening level, S_{open}, is defined as the applied load level at which all the compressive residual stresses in the wake of the crack have been overcome.

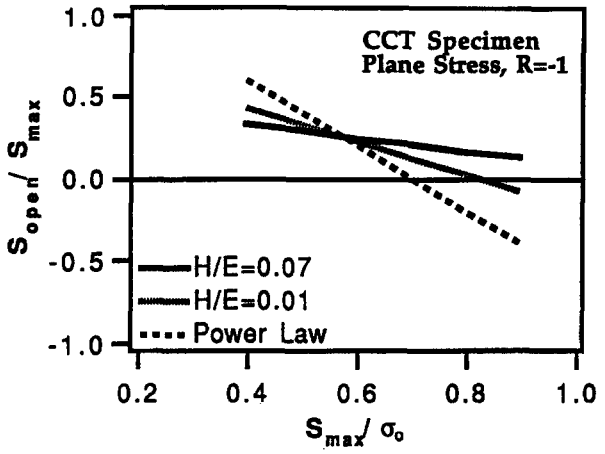

Figure 2. Variation of crack opening stress with $S_{\max}/\sigma_0$ and H/E.

3. The effect of $S_{\max}/\sigma_0$ and H/E on closure

The influence of the maximum applied stress on the crack opening results has been well documented based on Dugdale models [8–9] and finite element simulations [21–23, 28]. The results from our finite element model (FEM) simulations are summarized in Figure 2.

The results are for long cracks in the CCT specimens and demonstrate that the normalized crack opening levels decrease with increasing $S_{\max}/\sigma_0$ ratio. The trends based on the different H/E ratios is also noteworthy. Originally, the model with $H/E = 0.07$ and the power law hardening model were both used to simulate material behavior of 1070 steel. Therefore, the difference between stress strain curves from these hardening models was very small. However, the difference of opening levels from these two materials was significant. There are several important reasons for the different behavior observed in these cases. As revealed in systematic studies in [22–23], the crack opening behavior is a competition between the forward plastic deformation that is responsible for crack opening and the reversed plastic deformation that is responsible for the residual displacements. The bilinear response does not permit ratchetting of strain or mean stress relaxation under load control cycling while the power law representation does. Consequently, the maximum strains and mean strains at the crack tips for these models are different, resulting in different closure behaviors. In Figure 3 the stress-strain behavior of a material as the crack tip approaches and reaches it are shown. Initially when the crack tip is far from the material point the behavior is elastic and as the crack tip approaches the material point plastic strains accumulate. We note that the details of the $\sigma - \varepsilon$ representation have a considerable influence on the strain range, the stress ranges and the mean values of strain and stress. In this case at $S_{\max}/\sigma_0 = 0.7$ the power law representation provides the highest accumulated strain levels.

4. Notch effects on crack closure

It has been observed experimentally that fatigue cracks growing from a notch may grow at unusually high crack growth rates when the crack length is much smaller than the notch width [8, 51–57]. These small cracks propagate initially at high crack growth rates, decelerate to a minimum rate, and then match the long crack data trend. This period is crucial since a

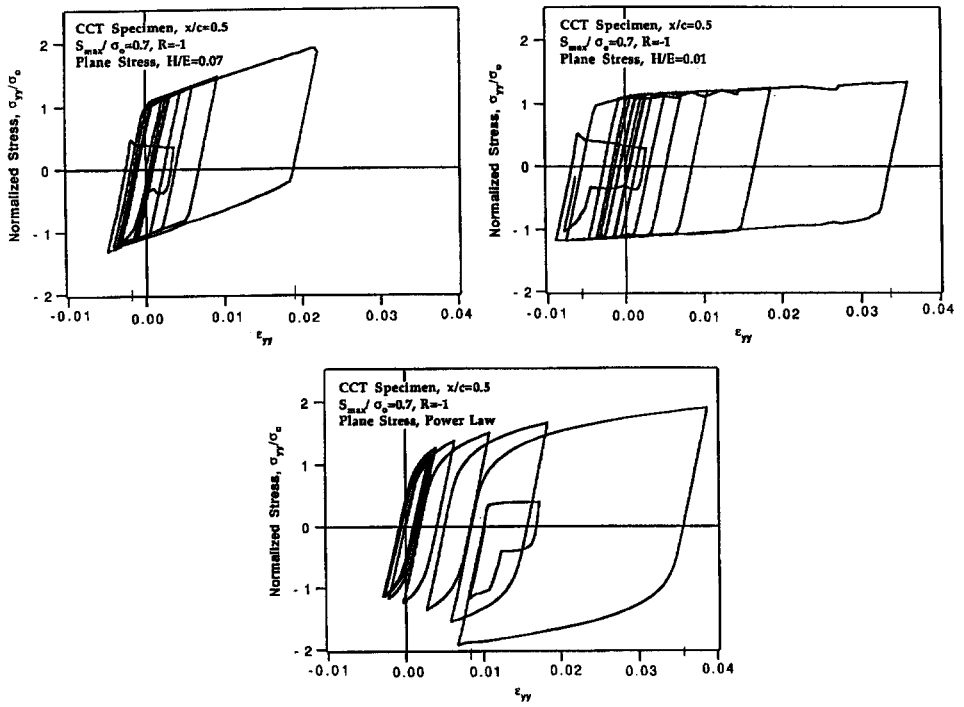

Figure 3. Stress-strain response of a material point as the crack tip approaches it and reaches it. The three plots correspond to different hardening models which simulate plane stress conditions under $R = -1$ loadings.

considerable fraction of the crack propagation lifetime could be spent in the regime where transient changes in crack growth behavior occur. One explanation of the accelerated crack growth rate at notches is based on crack closure concepts. When a crack initiates from a notch root, the plastic wake field is not fully developed. As the crack grows, the plastic wake develops and the crack tip generates its own stress fields which dictate the closure behavior, causing the influence of the notch to become gradually smaller.

Sehitoglu [57] proposed a model of crack closure for cracks growing from notches. The model accounted for crack length, applied stress and R-ratio effects. The model predicted the gradual increase in the crack opening load as the crack advanced from the notch root, and transient changes in opening level even when the notch root plasticity is absent. As with other Dugdale type models, the limitation of the model has been the plane stress deformation, and elastic-perfectly plastic idealization of material behavior. There are other models for crack growth from notches [57–66] including the works of Sehitoglu and Leis in the US, Miller et al. in the UK and Nishitani and Tanaka in Japan. The data indicates that accelerated crack growth rates occur well beyond the notch plastic zone. Therefore, notch plasticity alone can not account for accelerated growth rates.

An equation ((3) – Table 1) which relates the crack opening stress to the crack length, stress concentration factor of the notch, applied load magnitude and the R ratio was proposed based on the finite element results. Constants A, B, D are dependent on R, K_t and elastic stress concentration factor of the notch. Results are given in Table 1. The prediction equation is the same for $H/E = 0.07$ and 0.01, but the expression for $S_{\text{open}}^{\text{stable}}/S_{\max}$ and constants, A, B, and D are different.

Table 1. Summary of the crack closure simulations for crack growth from a notch

$H/E = 0.07$, plane stress	$H/E = 0.01$, plane stress
$\frac{S_{open}^{stable}}{S_{max}} = 0.49 + 0.01R - (0.1 - 0.3R)\frac{S_{max}}{\sigma_0}$	$\frac{S_{open}^{stable}}{S_{max}} = 0.95 + 0.13R - (0.70 - 0.30R)\frac{S_{max}}{\sigma_0}$
$A = -0.255 - 1.375R + (0.085 - 0.075R)K_t$	$A = -1.138 - 1.138R + (0.163 + 0.163R)K_t$
$B = 0.298 + 0.563R + (-0.043 - 0.198R)K_t$	$B = 0.902 + 0.507R - (0.089 + 0.164R)K_t$
$D = 1.700 + 1.475R + (0.100 - 0.225R)K_t$	$D = 3.400 + 2.575R - 0.125R\,K_t$
6	6
$F = \exp(-10 \times l/c)$	$F = \exp(-10 \times l/c)$

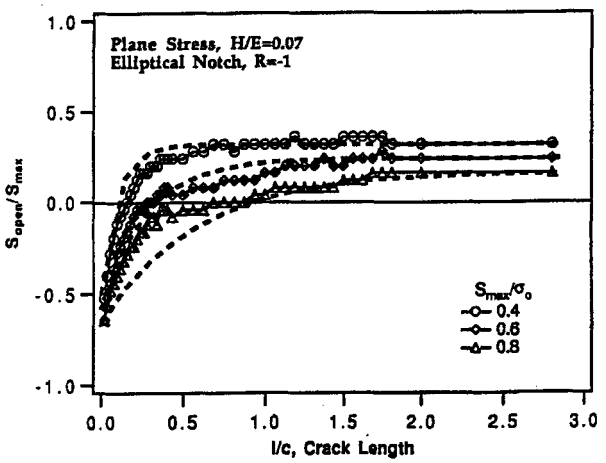

Figure 4a. Comparison of the transient closure levels determined by FEM and using Table 1.

$$\frac{S_{open}}{S_{max}} = \left\{ \frac{S_{open}^{stable}}{S_{max}} - \left[A\left(\frac{S_{max}}{\sigma_0}\right) + B \right] \times \exp\left[\frac{-l/c}{\left(\frac{S_{max}}{\sigma_0}\right) D} \right] \right\} (1 - F) + FR \qquad (3)$$

The predicted crack opening stresses match the finite element results very closely as shown in Figure 4(a). The dashed lines indicate that opening stress levels reach the stable value of $S_{open}^{stable}/S_{max}$ as l/c becomes large. The stable value of S_{open} is dependent on both R-ratio and S_{max}/σ_0.

Sehitoglu tested crack growth rate from a blunt notch ($K_t = 5$) under different applied stress levels. The crack growth equation constants C' and m' were equal to 8.03×10^{-9} and 3.202, respectively, and a bilinear relation with $H/E = 0.07$ was used. The results are shown in Figure 4(b). The notch plastic zone size, r_p, is also indicated in this figure. The long crack growth rate was predicted by using $S_{open}^{stable}/S_{max}$, and the short crack growth rate was predicted by using S_{open}/S_{max} ((3) in Table 1). The short crack growth rates were much higher than the long crack growth rate. Transient changes in the crack growth behavior and gradual linking with the long crack growth data occurred outside r_p. Also, the minimum in da/dN occurred at a crack length outside the plastic zone of the notch.

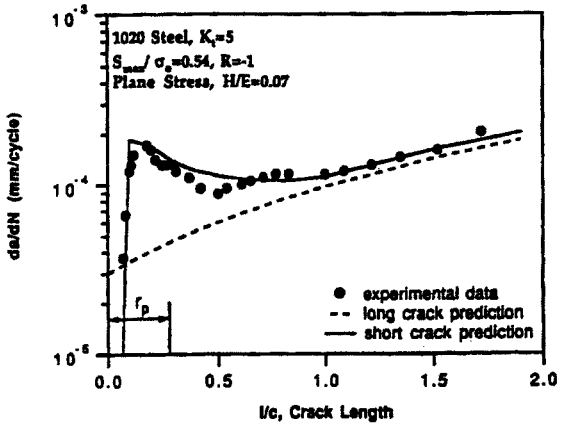

Figure 4b. Comparison of prediction and experiment 1020 Steel $S_{\max}/\sigma_0 = 0.54$, $K_t = 5$.

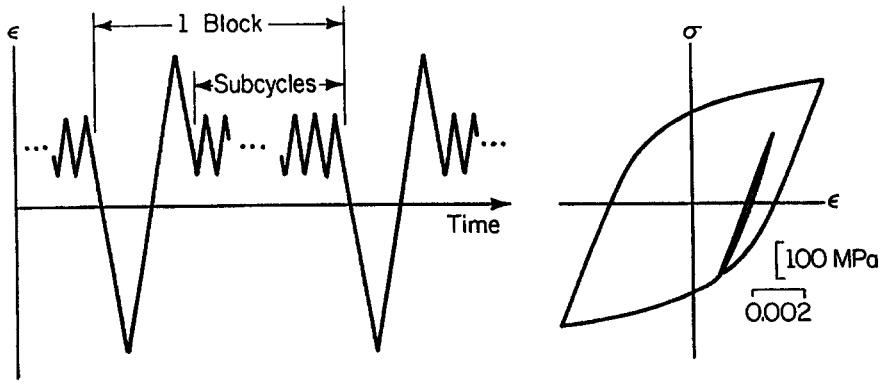

Figure 5a. Schematic of the block loading history [7].

5. Variable amplitude effects

It is expected that in the presence of overloads, subcycles within a major cycle, or load shedding cycles (such as in threshold testing produces) considerable transient changes in closure levels will occur. The increase in closure levels due to single overloads has been well documented [67]. Another important, yet not widely known effect, is the 'acceleration' of fatigue cracks under small amplitude cycles when they occur following a large amplitude cycle. These results are shown in Figures 5(a)–5(b).

In Figure 5(a) the strain history is shown. There are one hundred subcycles per block. The subcycles are applied during the unloading portion of the major cycle. Because the closure level is a function of $S_{\max}/\sigma_0$, the higher amplitude cycle has a much lower closure level than the subcycle. During the subcycles the crack remains fully open until it develops its own wake. If the subcycles were applied in isolation their closure level would be high, hence the crack growth rate under constant amplitude small cycle loading would be very slow. The prediction of crack growth in the absence of closure correction is given by the dashed line in Figure 5(b). The solid line is the prediction using the model developed in [16] and explained further in [7] for this case. The improvement in the crack growth rate prediction is remarkable.

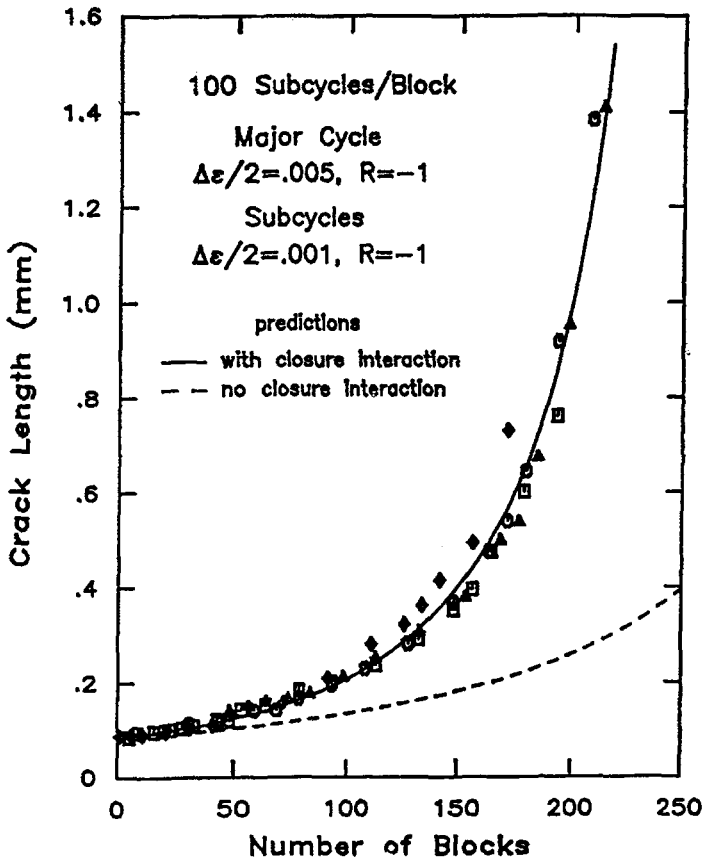

Figure 5b. Comparison of experimental and predicted crack growth rates under simple block histories [7].

6. The role of stresses ahead of the crack tip

Many closure studies placed attention on residual stresses behind the crack tip, and the applied load level required to overcome these residual stresses has been identified as the crack 'opening' load [6, 22–23, 28]. However, compressive stresses could be present ahead of the crack tip when the cracked body is at the 'opening' load and further loading increments are required before these stresses become tensile. This problem advocates the definition of several new crack opening parameters. The applied stress (load) at which the crack tip becomes tensile is defined as $S_{tt}(P_{tt})$, and the applied stress (load) at which all of the compressive stresses in the uncracked ligament become positive is defined as $S_t(P_t)$.

The residual stresses at the crack tip evolve from two contributions: (i) residual stresses due to 'constraint' at the crack tip in the absence of crack closure effects, and (ii) residual stresses arising from crack face contact. In the absence of crack face contact, the residual stresses at the crack tip develop from (i) only. Hence, one may see a dependence of crack growth on the R-ratio, stress state, and prior stress history, even when crack closure [37, 68–73, 39–40] is considered to be small. For example, consider the case where the crack is subjected to tensile loading ($R = 0$). Upon initial unloading to zero stress, a residual compressive stress develops at the crack tip. The magnitude and sign of this residual stress zone depend on the crack tip blunting, material properties, and out of plane constraint, effects normally thought to exist

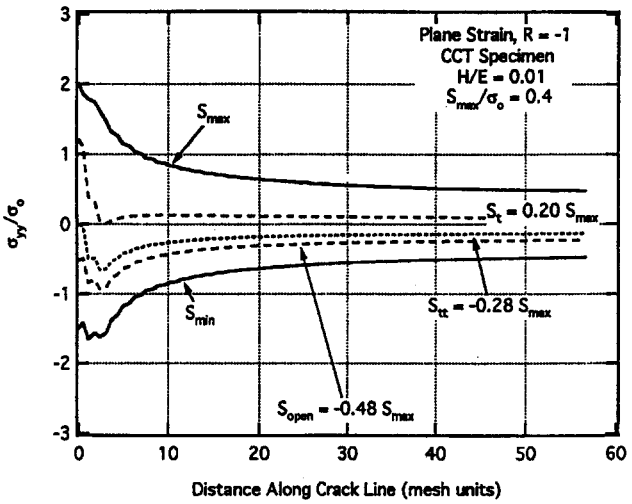

Figure 6a. Stress distribution near the crack tip at minimum load, at stress corresponding to tensile stress at crack tip, and maximum stress in plane strain for the CCT specimen.

exclusively in the presence of premature crack closure. The applied stress has to be increased to as much as 30% of the maximum stress level before these residual stresses are overcome. If the effect of crack contact is present, these two effects, (i) and (ii), will both play a role in governing crack growth. Note that residual stress due to (i) and (ii) are not independent, and experimental measurements will yield the combined effect. Careful numerical studies can isolate these two effects as discussed below. By studying the stress fields for 'stationary' cracks versus fatigue cracks, a distinction can be made between these two effects. These issues were considered by Sehitoglu and colleagues [30, 35, 41] who showed that residual stresses ahead of crack tips are more significant than stresses developed in the wake in plane strain loading.

To illustrate the above points, simulations are shown in Figures 6(a) and 6(b) for $R = -1$ loading with a crack growing from the notch in the CCT specimen under plane strain conditions. In Figure 6(a) it is noted that the crack tip opens at $S_{\text{open}} = -0.48 S_{\max}$ while it does not experience tensile stress until the load reaches $S_{\text{tt}} = -0.28\, S_{\max}$. The applied stress has to reach $S_t = 0.2\, S_{\max}$ before all the compressive stresses ahead of the crack tip are overcome. In Figure 6(b) the crack tip opens early for small cracks growing from notches (circle points) but the crack tip condition remains compressive until the load is increased further (triangular points). To overcome all of the compressive residual stresses in the uncracked ligament the applied stress has to be increased even further (rectangular points). These results could be used in development of more refined models of fatigue crack growth accounting for residual deformations, stresses and strains at crack tips. At the moment, the only correction that has been widely accepted is the ΔK_{eff} concept. This difference between S_{tt} and S_{open} is particularly significant under transient loading conditions, such as crack growth influenced by the presence of micro notches or crack growth under variable amplitude loadings. Under 'steady state' conditions the S_{tt} and S_{open} levels are similar to those in the CCT specimen.

In the early studies on crack closure in CCT specimens, the crack opening levels for plane stress were higher than for plane strain at low $S_{\max}/\sigma_0$ values, while at high $S_{\max}/\sigma_0$ levels

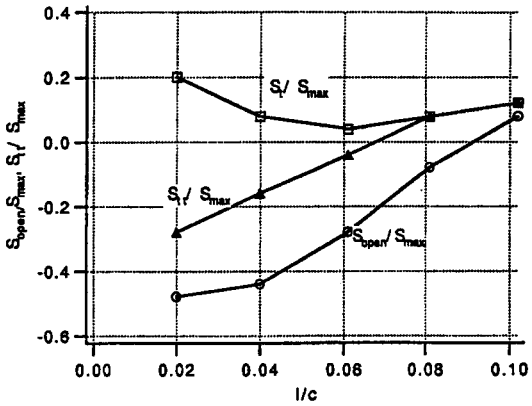

Figure 6b. Plot of $S/S_{\max}$ versus l/c for a crack growing from the notch root in CCT for $R = -1.0 K_t = 7$, plane strain, $S_{\max}/\sigma_0 = 0.4$.

the crack opening stress level for plane stress were lower. Both Newman [28] and Sehitoglu and colleagues [6, 21–23] reported such results. These results are correct but have not been fully understood until the studies of Sehitoglu and colleagues [30, 74]. They can be explained as follows. The residual displacements at the crack surfaces, proportional to the plastic strains in the thickness direction in plane stress and to the plastic strains in the transverse direction in plane strain, are higher in plane stress than in plane strain. Hence, the crack closure levels (which are directly proportional to the magnitude of the residual displacements along the crack line) should always be higher in plane stress compared to plane strain. However, at high $S_{\max}/\sigma_0$ levels, the curves switch because considerable crack tip blunting is observed in the plane stress case versus the plane strain case. This is illustrated in Section 9 through Figure 11(b).

7. Modeling of crack closure within a grain

As a crack traverses through the first few grains, depending on the orientation of the crack plane with respect to the crystallographic orientation, alternating slip bands at the crack tip can be inclined at different angles with respect to crack growth direction. Results from Neumann [47, 78, 79] showing the activation of slip systems at the crack tip are given in Figure 7(b). Previous slip lines were etched out to demonstrate that active slip occurs exclusively at the crack tip. Note that two macroscopic slip planes at the tip are active and that a slip free triangular zone forms. Despite this background of local slip at the microscopic level, the current models of fatigue crack growth have relied on a description of crack tip stress fields assuming plastic isotropy. For example, the models of fatigue crack closure, both semi-analytical models such as that of Dugdale and numerical models using finite element techniques have assumed plastic strain descriptions which are independent of crystallographic slip orientation. Consequently, no quantitative description of the local orientation effects on fatigue crack growth has been proposed. The 'original' FEM [21–23], which was based on isotropic material properties was modified for microscopic double slip [42, 44]. The plastic constitutive relationship is based on a plane strain double slip plane model proposed by Asaro and coworkers [75] (Figure 7(a)). Plastic deformation occurs exclusively along two slip planes which are characterized by unit vectors (s_1, m_1) and (s_2, m_2). The vectors are trigonometric functions of the two angles in

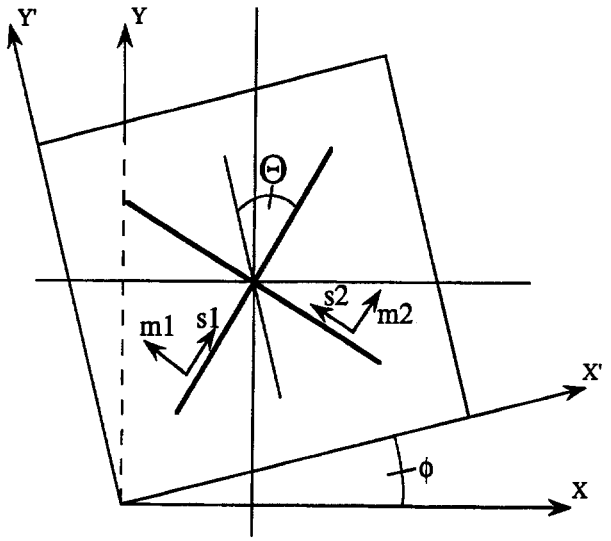

Figure 7a. Geometry of the in plane double slip model.

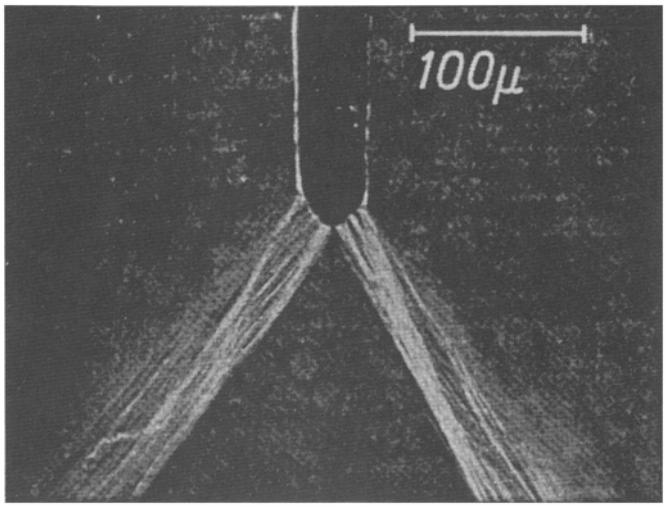

Figure 7b. Photograph of the crack tip region displaying localized slip (after Neumann, [47]).

Figure 7(a). The angle between either slip plane and the Y-direction of the crystal is denoted θ, and the orientation of the crystal with respect to the X-direction is denoted ϕ. Both slip directions and slip plane normals lie in the plane of the drawing. Plastic shear strains develop when the resolved shear stress on either slip plane reaches a critical value, defined as:

$$\lambda^{(\alpha)} = |\lambda_0 - \sigma_c^{(\alpha)}| \tag{3}$$

where λ_0 is the critical resolved shear stress and $\sigma_c^{(\alpha)}$ is the back stress on the slip plane. The back stress is calculated during plastic flow through

$$\sigma_c^{(\alpha)} = c'\gamma^{(\alpha)} \tag{4}$$

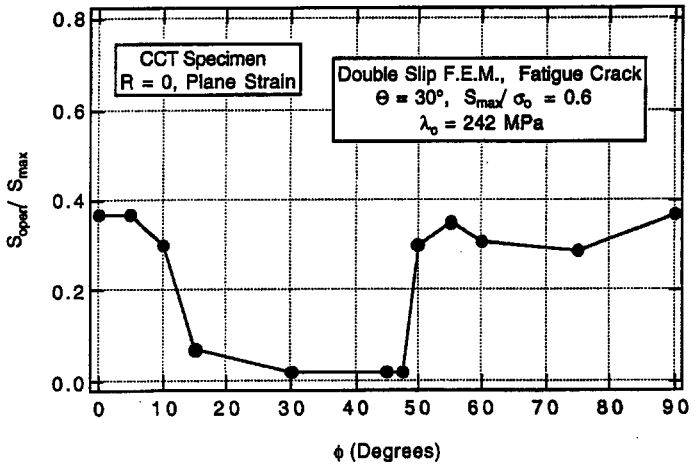

Figure 8a. Crack opening levels as a function of the crystallographic orientation of the slip systems, ϕ, for the center cracked tension specimen [42].

where c' is a constant in this hardening model, and $\gamma^{(\alpha)}$ is the current shear strain on a slip plane. The macroscopic slip is calculated by averaging the microscopic slip at every Gauss point in the mesh.

This model has been successfully used to model the tensile deformation of both BCC and FCC crystals [75], and later to study stationary cracks [76]. A more detailed description of the constitutive relation used to model the double slip phenomenon has been discussed [42–44]. The matrix that relates the shear stress rate to the shear strain rate for a given slip system, in our case assumes that latent hardening does not exist, i.e. slip on the primary plane does not cause hardening on the conjugate plane [77]. The strains are calculated using small deformation theory (additive strains). This representation is accurate for fatigue crack growth studies where the strain ranges at crack tips are not large [22–23].

The simulations are shown in Figures 8(a) and 8(b) for $R = 0$ conditions with $S_{\max}/\sigma_0 = 0.6$. For some crystallographic orientations, ϕ, the closure levels are found to be negligible, while in others the levels approach 0.35 $S_{\max}$. When varying the angle between the slip planes, Θ, the closure values span a similar range. The results are symmetric with respect to $\Theta = 45°$. The results have implications in describing crack growth and threshold stress intensity values when the crack traverses through grains of different orientations. These differences in closure stress levels can be used to rationalize the problem of variability in microstructurally short fatigue crack growth rates [43].

8. Effect of crack roughness and micro-contact on crack closure

The objective of this section is to gain more knowledge and insight about the roughness induced crack closure phenomenon. Since plasticity induced closure is well understood, it seemed essential to look at the roughness effects alone. The simulations were conducted under conditions where roughness induced crack closure is suspected to be the main contributor to closure.

Increases in slip planarity and the slip length enhance the roughness of crack surfaces. In these cases, asperity sizes (roughness levels) can be higher than the crack opening displacement [80–84] and roughness induced crack closure (R-ICC) is expected to significantly

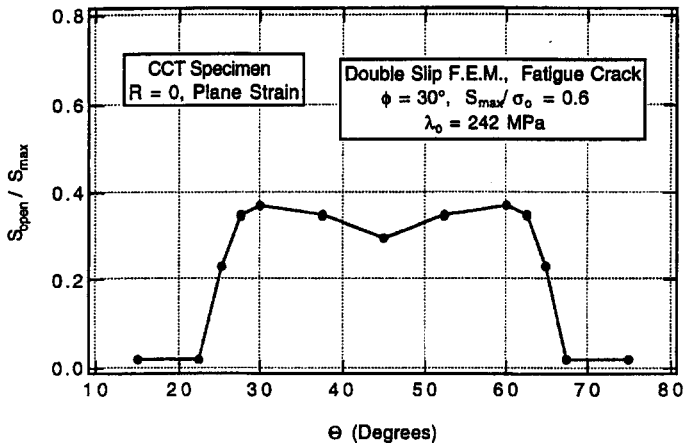

Figure 8b. Crack opening levels as a function of the angle between the slip systems, Θ, for the center cracked tension specimen [42].

influence crack growth behavior exceeding plasticity-induced closure effects. The titanium microstructures [20] (both the dual phase lath and equiaxed structures) exhibit rough crack paths and some experimental crack closure data has been documented on these alloys. No robust models have been forwarded to predict R-ratio and maximum stress effects. Previous models of crack advance have treated cracks with a triangular profile as described by a wedge angle and asperity height [85–87]. On the other hand, the real cracks exhibit a random roughness profile which can be described by a Gaussian or other type of distribution of heights and the surfaces can not be characterized by average surface roughness value alone.

It is generally accepted that upon deviating from a straight path, the crack faces are displaced in the direction parallel to the crack growth. This deviation results in a mismatch of the crack surfaces [83–87]. Therefore normal and sliding displacements must be considered for a non-straight crack, even when the remote loading is nominally of mode I type. Furthermore, since the rough fracture surfaces are undergoing repetitive loading, plastic flow of asperities must also be accounted for. In the limiting case, the asperities may deform and carry the load elastically, thus reaching a 'shakedown' state. A model, which accounts for these characteristics, has been developed for predicting and quantifying roughness induced crack closure [45]. This model is briefly reviewed below.

The crack opening stresses were calculated by solving an elastic problem which in turn involved the superposition of two other elastic problems: a center crack in a plate under uniform remotely applied stress, and a partially loaded crack where the loading is due to contact stresses. The crack is allowed to advance under either $K_{\max}$ = constant or $S_{\max}/\sigma_0$ = constant conditions. Near the crack tip, mode I and mode II loading conditions exist due to mismatch of crack surfaces. This is taken into account by analyzing sliding of the asperities, instead of solely looking at normal contact. The crack was subdivided into a finite number of strips. Each 'strip event' is treated as a contact problem between two randomly rough surfaces (Figure 9(a)). A close view of strip at location x_i is shown with corresponding separation distance, d_i. The separation distance, d_i., between two rough surfaces is equivalent to the crack surface displacements. Furthermore if the surface roughness was zero, d_i would be the COD in classical fracture mechanics. Figure 9(b) is a close-up view of the contact region defining the key parameters in roughness induced crack closure research. These parameters

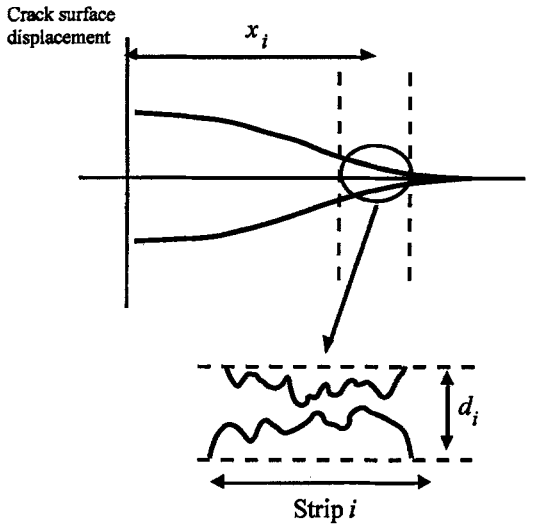

Figure 9a. Strip event used in R-ICC model.

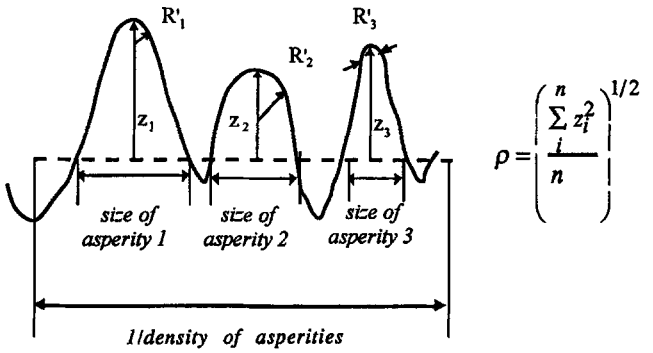

Figure 9b. Illustration of topographical parameters (n = number of asperities).

are asperity heights, asperity radii and the density of asperities. The local characterization is based on the statistics of the rough surface.

In the problem of R-ICC the 'unit event' is one of two asperities which undergo sliding (mode II) displacements. The behavior of individual asperities in sliding contact has been determined by Johnson-Shercliff [9]. Furthermore, their analysis (as well as the R-ICC model) assumed that asperities deform plastically and reach a shakedown state where further deformation is elastic. Incorporating this unit event into the statistics of contact [88–91] leads to a load-separation distance relationship. Greenwood and Williamson [88] studied the elastic contact of nominally flat surfaces. They employed Hertzian contact equations to describe individual asperity behavior (i.e. the unit event) and then by defining the *probability of contact* between two surfaces the load carried over a randomly rough surface was obtained. By equating the contact load to the residual contact stresses developed during fatigue, the opening levels to overcome these stresses can be determined.

Each surface is characterized by an initial normal asperity height, ρ, a constant asperity tip radius, R', and a constant density of asperities, n. The model is not restricted to a particular height distribution, however the assumption of a Gaussian height distribution was reasonable

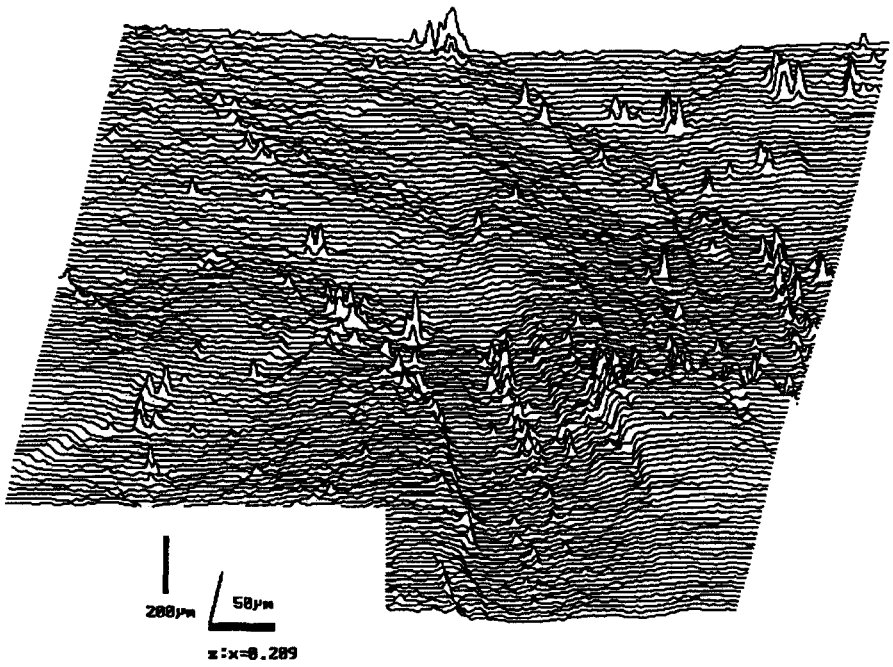

Figure 9c. Topography of crack surfaces for Ti based alloy.

[88] and confirmed by confocal microscopy (Figure 9(c)) for the fracture surface of TiAl. The average surface roughness, ρ, in this case is $40\,\mu$m. After repeated contact the distribution changes as plastic flow of asperities occurs.

Plasticity induced closure is not allowed in the model in order to isolate and focus on the roughness effects. The results are highly sensitive to ρ, R', n, material properties such as yield strength strain hardening, shakedown pressure which is related to shear to normal traction ratio (Q/P), where P represents resultant normal force due to contact, and Q is the tangential component. Dependng on the Q/P ratio the shakedown pressure, p_0^s, may be $2(Q/P = 0.6)$ to $4(Q/P = 0)$ times the shear yield strength, k. [89].

Simulations were conducted for crack opening stresses under plane strain conditions. The crack opening stress definition remains the same as before, i.e. it is defined as the stress level at which all compressive residual stresses (arising from contact) are overcome. Results of simulations are shown in Fig. 10(a) and 10(b). In Figure 10(a) the maximum applied stress was $S_{\max}/\sigma_0 = 0.44$ and the number of cycles was 100. The mean roughness was 30 microns and the initial K was $10\,MPa\sqrt{m}$. As the number of asperities per unit length increases the crack opening levels also increase. Also, as the crack size increases the $S_{\text{open}}/S_{\max}$ ratio gradually decreases.

The ρ/R' ratio provides a more complete picture of the 'average' asperity. In the case of the asperity density remaining constant, ρ/R' corresponds to a sense of height vs. size and fully encompasses the effect of the surface's topography. Since C is constant, (a non dimensional measure of the deformation of asperity profiles given by, $[p_0^s/E]^2[2\ln(4E/p_0^s - 1)]$ where p_0^s is the shakedown pressure and E, Young's modulus [45]) increasing ρ/R' ratio will increase the opening loads (Figure 10(b)). This results from the fact that as the ρ/R' ratio increases, a greater number of asperities will make contact.

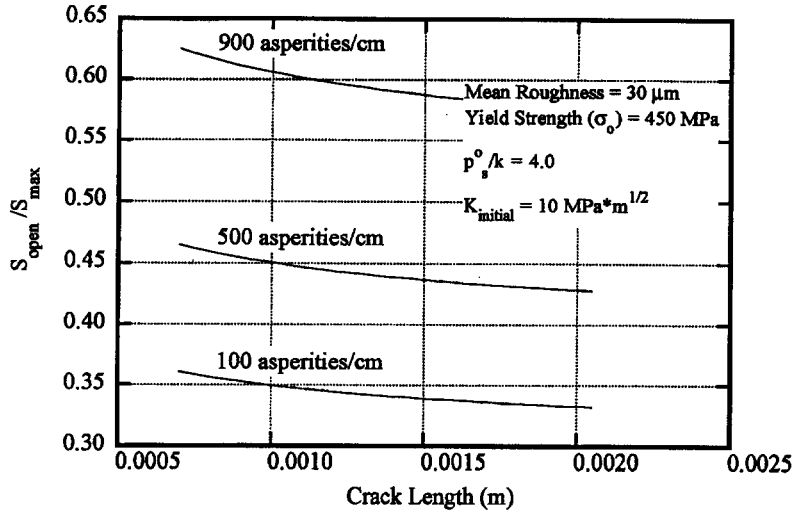

Figure 10a. Crack opening stress vs. crack length variation with surface density of asperities. R-ratio = 0.1, $S_{max}/\sigma_0 = 0.44$.

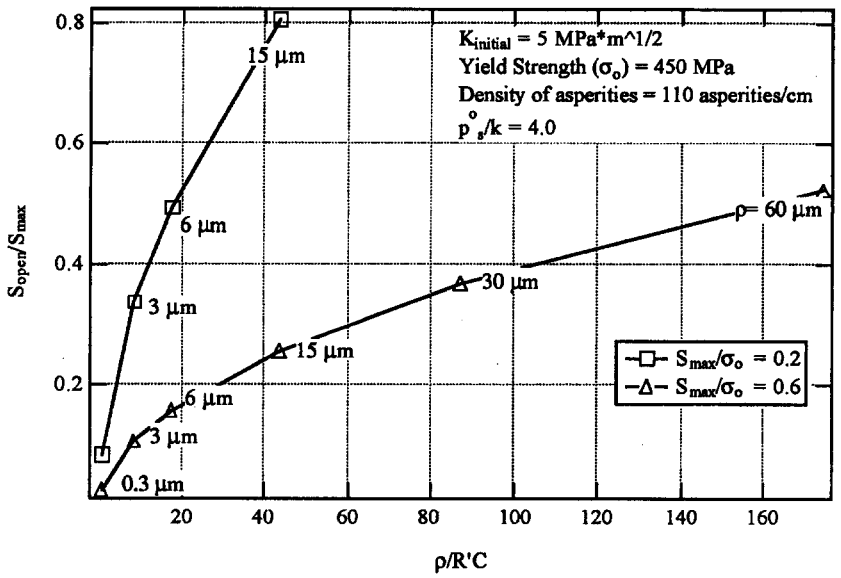

Figure 10b. Crack opening stress as a function of normalized roughness and S_{max}/σ_0.

Also shown in Figure 10(b) the crack opening stress is a function of ρ, for the case of R', the mean radius at the tip of the asperities, remaining constant. We note the dramatic effect of ρ and S_{max}/σ_0 on the results. In this simulation initial maximum stress intensity of 5 MPa$\sqrt{m}$ and a constant asperity density of 110 asperities per cm were chosen.

The model verifies that a fuller topographical description, where the size, density and sharpness of asperities are characterized is necessary to predict the roughness effect. Thus it is probably useful to specify non-dimensional parameters that include topographical and material properties, which would more clearly define 'roughness' as it pertains to the R-ICC phenomenon.

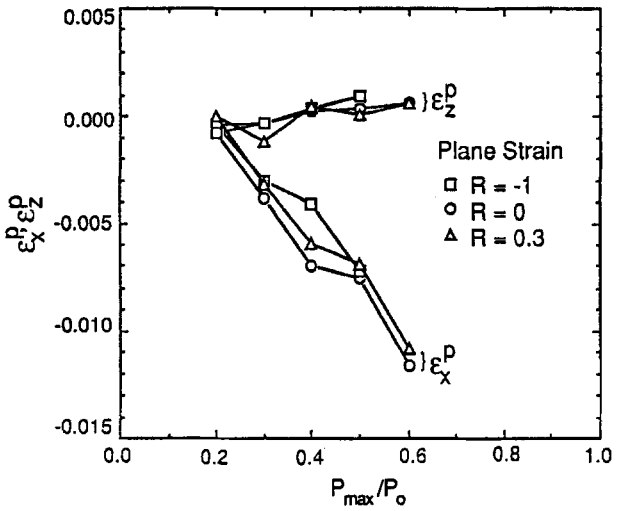

Figure 11a. Plastic strain components in plane strain fatigue crack growth sumulations.

9. Out-of-plane and in-plane constraint

There has been considerable debate over whether crack closure occurs under plane strain (out-of-plane constraint) conditions [10, 11, 25, 33, 39, 40]. Experimental results of Fleck [16] on CT specimens, using the push rod technique, confirm the presence of closure in plane strain. Numerical solutions showed results on crack closure under plane strain [12, 13, 22–23, 30, 33, 35, 41]. These numerical results showed that in the plane strain case the wake contact zone is small and located very near the crack tip, therefore, remote measurements could not capture plane strain crack closure. Sehitoglu and Sun [35, 41] proposed that contraction of the material at the crack tip in the x-direction (along the crack growth direction) is responsible for closure in plane strain. This was confirmed by considering the displacements in the x-direction relative to the crack tip as well as by determining the ε_x^p component of strain at the crack tip as shown in Figure 11(a). The ε_x^p component of strain is compressive causing a permanent decrease in the ligament size in the x-direction ahead of the crack tip. Upon crack advance, this element will unload and will produce residual material on the crack surfaces. Figure 11(a) demonstrates that the ε_z^p component only has a small contribution to crack closure levels, contrary to the plane stress case.

Since the mechanism is different, the crack closure levels are different under plane stress and plane strain. Normalized crack opening loads, $S_{\text{open}}/S_{\text{max}}$, as a function of maximum stress normalized by the flow stress, S_{max}/σ_0, are presented in Figure 11(b) for the $R = -1$ case. At low applied stress levels the opening loads for plane strain are lower than those for plane stress. The results indicate that the $S_{\text{open}}/S_{\text{max}}$ decreases with increasing maximum stress, and the opening stress enters the compressive regime at S_{max}/σ_0 levels beyond 0.6 for plane stress and 0.8 for plane strain. We note that these results hold for the $H/E = 0.01$ case. Similar results have been reported for the CT specimen if the loads are normalized by the limit load. Based on residual displacements the closure levels in plane strain should always be lower than the plane stress values. The exception to this is at high S_{max}/σ_0 levels, where the plane stress case demonstrates a more blunt crack tip relative to the plane strain case.

These results are consistent with experimental results reported by Allison et al. [25], Vasquez et al. [92–93], and the survey conducted by McClung [94] confirming the nearly

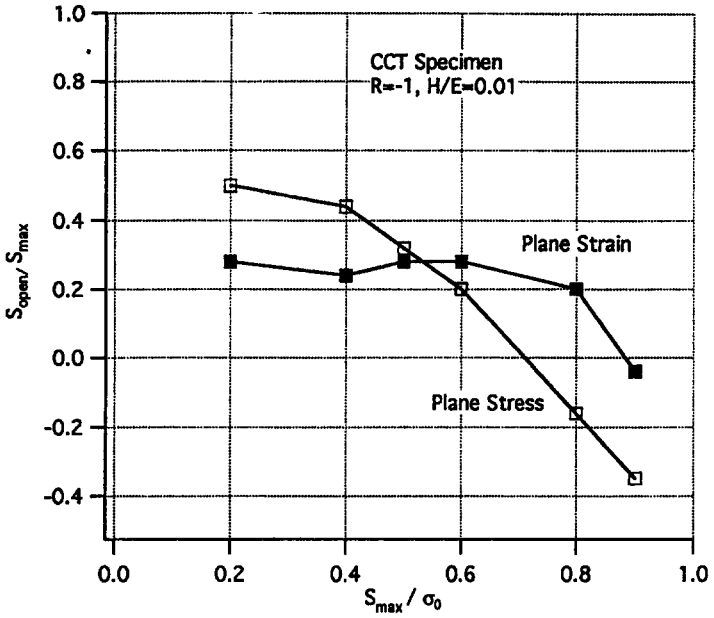

Figure 11b. Fatigue crack opening loads in the case of plane stress versus plane strain.

constant S_{open} levels observed in the experiments. At high crack growth rates, or when the net section stresses approached the yield strength, the experimental S_{open} levels decreased with increasing crack length as noted in the data by Fleck [40] and Staal and Ellen [95]. As a first order approximation one may interpret $S_{\max}$ as the net stress (load/uncracked ligament).

The in-plane constraint [96–97] can be most conveniently studied by considering a mode I crack and varying the magnitude and direction of the applied stress level parallel to the crack, $S_x(S_y = \text{Constant}, S_z = 0)$. The cruciform geometry used to study this phenomenon is shown in Figure 12(a). Three ratios of $\lambda = S_x/S_y$ have been considering including $\lambda = 0$ tensile loading, $\lambda = -1$ pure shear loading, and $\lambda = 1$ equibiaxial loading. The results (Figure 12(b)) show that crack closure levels are lowest for the $\lambda = -1$ case and highest for the $\lambda = 1$ case with $\lambda = 0$ the results lying between the two. These results can predict the experimentally observed crack growth behavior reported by Brown and Miller [98]. The capability of the model to predict the crack growth rates obtained from cruciform specimens is shown in Figure 12(c). The model predicts the highest crack growth rate for the $\lambda = -1$ case. We note that the hydrostatic stress, σ_H, is zero in the $\lambda = -1$ case, while $\sigma_H > 0$ for the $\lambda = 1, 0$ cases.

10. Crack closure under time dependent loading

Crack closure behavior is considerably influenced by the presence of hold periods at elevated temperatures [50]. Tensile hold periods increase the crack tip stretching, in turn reducing crack closure levels and increasing crack growth rates. The key parameters are the hold period, t_h, the creep exponent, m, and the creep constant, σ_c. The creep response and the plasticity response are depicted by the following equations:

$$\dot{\varepsilon}_{ij}^{c} = \frac{3}{2}\dot{\varepsilon}_c^0(\bar{\sigma}/\sigma_c)^{m-1}\frac{S_{ij}}{\bar{\sigma}} \tag{5}$$

$$\bar{\sigma}/\sigma_0 = (\overline{\varepsilon^p}/\varepsilon_0^p)^n \tag{6}$$

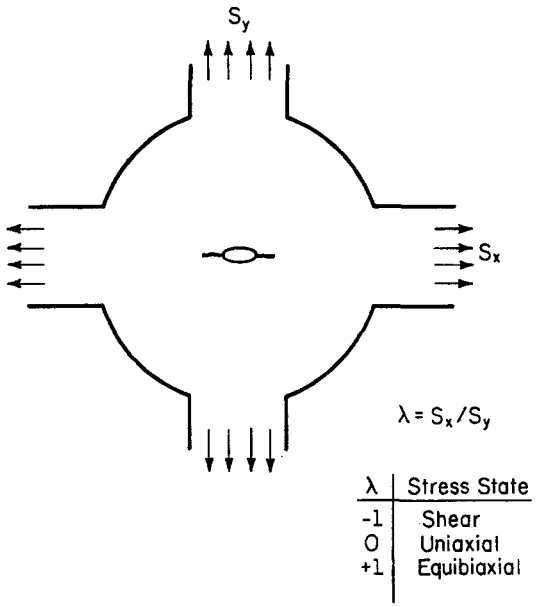

Figure 12a. Geometry used for in-plane constraint studies.

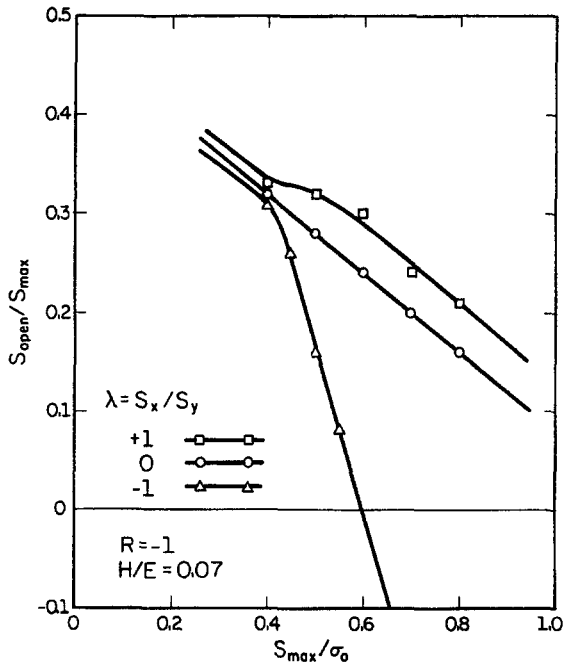

Figure 12b. Crack opening stress as a function of biaxiality ratio, λ[48].

An expression for effective stress ratio as a function of these parameters has been determined and shown with the FEM simulations in Figure 13(a). The creep exponent m is 5 and the horizontal axis is the ratio, σ_c/σ_0, while the vertical axis is the effective stress ratio, U, defined as $\Delta S_{\text{eff}}/\Delta S$. As $S_{\max}/\sigma_0$ increases, U increases for a constant σ_c/σ_0 ratio. The expression that fits these trends is shown in Figure 13(a) as an annotation, and also as (7).

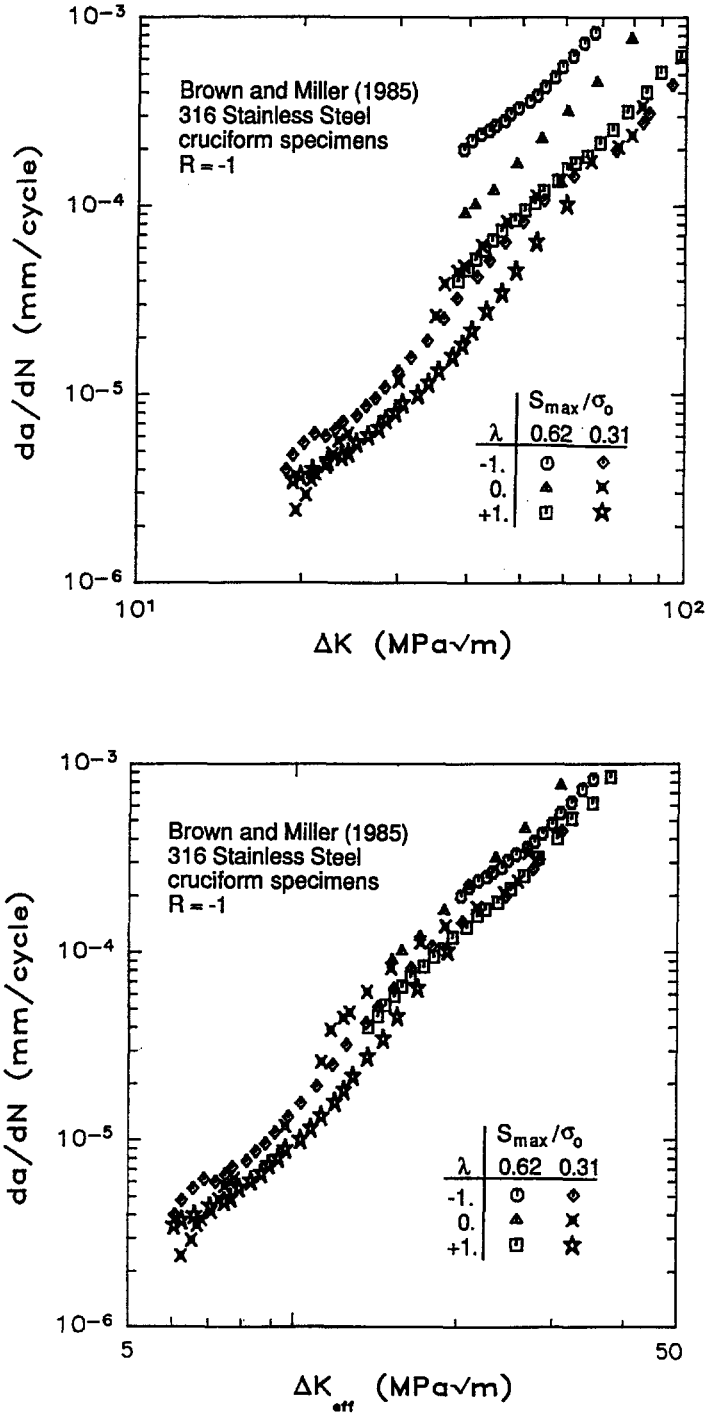

Figure 12c. Crack growth results of Brown and Miller exhibiting higher crack growth rates for the $\lambda = -1$ case and the consolidation of results using ΔK_{eff} [49].

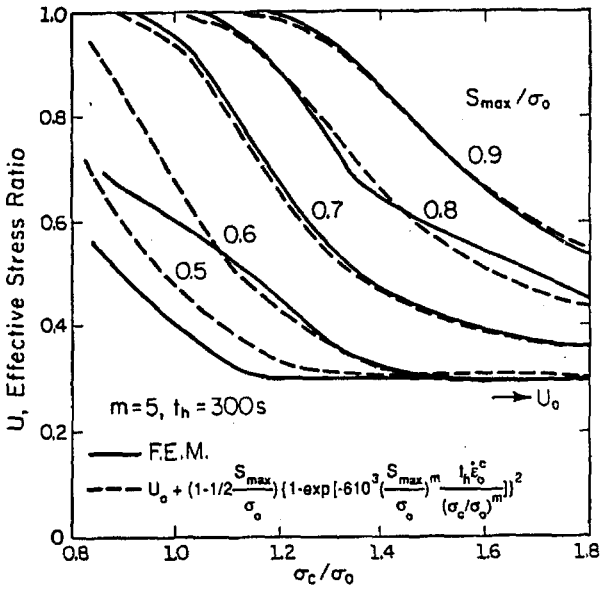

Figure 13a. Effective stress ratio as a function of maximum stress and the prediction with the U expression ($R = 0$ plane stress) [50].

The values for $n = 0.0816$ and $\sigma_0 = 993\,\text{MPa}$ were chosen to represent Rene 95 [50]. When σ_c/σ_0 becomes large or when hold time t_h is zero, the creep deformation becomes negligible and the results asymptotically approach U_0. The U_0 corresponds to the $S_{\max}/\sigma_0$ dependence of crack opening load under time independent conditions. The value of U_0 is around 0.3 for $S_{\max}/\sigma_0 \leqslant 0.6$ and $0.5\,S_{\max}/\sigma_0$ for $S_{\max}/\sigma_0 > 0.6$. The variation of U with the applied stress level, creep properties, and hold period is:

$$U - U_0 = \left(1 - \frac{1}{2}\frac{S_{\max}}{\sigma_0}\right)\left(1 - \exp\left[-6.10^{-3}\left(\frac{S_{\max}}{\sigma_0}\right)^m \frac{t_h\dot{\varepsilon}_0^c}{\left(\sigma_c/\sigma_0\right)^m}\right]\right)^2 \tag{7}$$

The crack closure results have been applied to fatigue crack growth in Rene 95. Since this material undergoes transgranular crack growth, no new damage mechanisms are introduced due to the hold period, and the crack closure model predicts hold period growth rate results effectively (Figure 13(b)).

11. Conclusions

1. The crack opening stress is a strong function of $S_{\max}/\sigma_0$, the strain hardening behavior (H/E), and the R loading ratio. The increase in $S_{\max}/\sigma_0$ can be viewed as decrease in 'elastic constraint' and results in a decrease in crack opening stress levels. The dependence of the opening stress on $S_{\max}/\sigma_0$ is stronger for plane stress cases relative to plane strain and also stronger for the case of $R = -1$ relative to $R = 0$. The crack opening stresses are a strong function of the plastic modulus (H/E ratio) or the power law strain hardening exponent. If the model permits mean stress relaxation and/or ratchetting under cyclic loading this will have an influence on the ensuing crack opening stress levels.

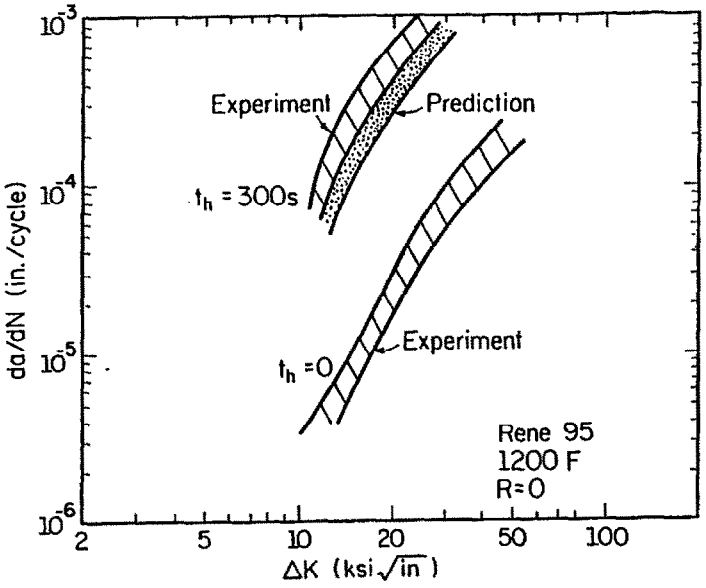

Figure 13b. Crack growth prediction for the Rene 95 under $t_h = 0$ and $t_h = 300$ seconds

2. The crack opening stress levels are as low as the minimum applied stresses when cracks start from notch roots, then they increase with increasing crack length until the stabilized values are reached. Crack closure is a main factor responsible for the notch effect on crack growth behavior. A set of equations was proposed to determine crack opening stresses when cracks grow from notches for variable notch shapes, applied maximum load levels, R ratios, crack length and different materials. The experimental results indicate that transient changes in crack growth rate were not limited to the notch plastic zone, as was predicted correctly with the model.

3. The crack closure concept can be used to predict crack growth for variable amplitude histories where large strain excursions have a major influence on crack opening behavior. The periodic application of major strain cycles can cause significant crack acceleration. Experiments and crack growth predictions are in excellent agreement.

4. Even when a fatigue crack opens, the stresses ahead of the crack tip could be compressive. Crack advance is expected when the crack tip stresses become tensile. Under transient loading conditions such as a crack growing from a notch, or under variable amplitude loading, the distinction between crack opening stress, S_{open}, and the applied stress at which the crack tip becomes tensile, S_{tt}, could become significant. Even in the absence of closure one would expect R-ratio, overload (and underload), and stress state effects because S_{tt} is dependent on these parameters.

5. By using a double slip plastic deformation finite element model, the variation of the crack opening stress levels as a function of orientation of the two microscopic slip planes is evaluated. For $R = 0$ plane strain conditions we found that the $S_{\text{open}}/S_{\max}$ ratio ranged from 0.4 to 0.05. This means that considerable transients in crack growth are expected as the crack traverses through the microstructure. Once the crack reaches a sufficient size, then closure levels corresponding to isotropic simulations would be appropriate.

6. Roughness induced crack closure depends on the height of asperities, their statistical distribution, their density and tip radius, and the material flow properties in compression. The

roughness induced closure model developed incorporates all these features, accounting for mode II sliding displacements and predicting crack opening stress levels that are in reasonable agreement with experimental findings.

7. Plasticity induced crack closure occurs in plane strain (out-of-plane constraint) and the residual material comes from contraction of the ligament in the crack growth direction. Closure levels in plane strain can in fact be higher than closure stress levels in plane stress at high S_{max}/σ_0 ratios. Decreasing the in-plane constraint (or hydrostatic stress) by applying a compressive stress parallel to the crack lowers the crack opening stress levels. The experimental crack growth rate results on cruciform specimens confirm this finding.

8. The presence of tensile hold periods at elevated temperatures decreases the crack opening stress levels and hence results in increased crack growth rates. The crack opening stress levels depend on the creep constants, the plastic strain relationship, the hold period, and the S_{max}/σ_0 ratio. The model predicts the crack growth rates in Rene 95 under hold time conditions.

Acknowledgments

The research is funded by the Fracture Control Program, College of Engineering, University of Illinois. The simulations were funded with grants from the National Center for Supercomputer Applications at University of Illinois over the last few years. The simulations were initially conducted using a CRAY-XMP48 supercomputer located in National Center for Supercomputer Applications at University of Illinois with execution times of 1 CPU hour per simulation and later on the Power Challenge Computers with similar execution times. The contributions of early research assistants including Paul Lalor (MS 1986), Craig McClung (PhD 1987), Wei Sun (PhD 1991) and Yavuz Kadioglu (PhD 1991) are acknowledged.

References

1. P. Paris, M.P. Gomez and W.E. Anderson, A Rational Analytical Theory of Fatigue, *The Trend in Engineering*, University of Washington 13 (1961) 9–14.
2. W. Elber, Fatigue Crack Closure under Cyclic Tension, *Engineering Fracture Mechanics* 2 (1970) 37–45.
3. W. Elber, The Significance of Fatigue Crack Closure, *Damage Tolerance in Aircraft Structures*, **ASTM STP 486** (1971) 230–242.
4. A.J. McEvily, On Crack Closure in Fatigue Crack Growth, *Mechanics of Fatigue Crack Closure*, **ASTM STP 982** (1988) 35–43.
5. D.L. Davidson, Fatigue Crack Closure, *Engineering Fracture Mechanics* 38:6 (1991) 393–402.
6. P. Lalor, H. Sehitoglu and R.C. McClung, Mechanics Aspects of Small Crack Growth from Notches — The Role of Crack Closure, *The Behavior of Short Fatigue Cracks*, EFG Pub. 1, Mechanical Engineering Publications, London (1986) 369–386.
7. R.C. McClung and H. Sehitoglu, Closure Behavior of Small Cracks under High Strain Fatigue Histories, in *Mechanics of Fatigue Crack Closure, ASTM STP 982* (1988) 279–299.
8. J.C. Newman, Jr., A Nonlinear Fracture Mechanics Approach to the Growth of Small Cracks, in *Proceedings of the 55th AGARD Meeting on Behaviour of Short Cracks in Airframe Components*, Toronto (1982).
9. J.C. Newman, Jr., A Crack-Closure Model for Predicting Fatigue Crack Growth under Aircraft Spectrum Loading, *Methods and Models for Predicting Fatigue Crack Growth under Random Loading*, **ASTM STP 748** (1981) 53–84.
10. H.L. Ewalds and R.T. Furnee, Crack Closure Measurement Along the Fatigue Crack Front of Center Cracked Specimens, *International Journal of Fracture* 14 (1978) R53–R55.
11. D.S. Mahulikar, W.P. Slagle and H.L. Marcus, Edge Effects on Fatigue Crack Closure of Aluminum Alloys, *Scripta Metallurgica* 3 (1979) 867–880.
12. A.F. Blom and D.K. Holm, An Experimental and Numerical Study of Crack Closure, *Engineering Fracture Mechanics* 22:6 (1985) 997–1011.

13. K. Ogura, Y. Miyoshi and I. Nishikawa, Fatigue Crack Growth and Closure of Small Cracks at the Notch Root, *Current Research on Fatigue Cracks*, MRS Vol. 1, Society of Materials Science, Japan (1985) 67–91.
14. W.N. Sharpe and X. Su, Closure Measurements of Naturally Initiating Small Cracks, *Engineering Fracture Mechanics* 30:3 (1988) 275–294.
15. H. Nisitani, and K. Takao, Significance of Initiation Propagation and Closure of Microcracks in High Cycle Fatigue of Ductile Metals, *Engineering Fracture Mechanics* 15:3–4 (1981) 445–446.
16. H. Sehitoglu, Crack Opening and Closure in Fatigue, *Engineering Fracture Mechanics* 21:2 (1985) 329–339.
17. J.E. Allison, R.C. Ku and M.A. Pompetzki, A Comparison of Measurement Methods and Numerical Procedures for the Experimental Characterization of Fatigue Crack Closure, in *Mechanics of Fatigue Crack Closure, ASTM STP 982* (1988) 171–185.
18. J.A. Vazquez, A. Morrone and H. Ernst, Experimental Results on Fatigue Crack Closure for Two Aluminum Alloys, *Engineering Fracture Mechanics* 12 (1979) 231–140.
19. J.A. Vazquez, A. Morrone and J.C. Gasco, A comparative Experimental Study on the Fatigue Crack Closure Behavior Under Cyclic Loading for Steels and Aluminum Alloys, in *Fracture Mechanics, ASTM STP 677* (1979) 187–197.
20. J.M. Larsen, The Effects of Slip Character and Crack Closure on the Growth of Small Fatigue Cracks in Titanium-Aluminum Alloys, Ph.D. thesis, Materials Science Department, Carnegie Mellon University, 1988.
21. P. Lalor and H. Sehitoglu, Crack Closure Outside Small Scale Yielding Regime, in *ASTM STP 982* (1988) 342–360.
22. R.C. McClung and H. Sehitoglu, Finite Element Analysis of Fatigue Crack Closure 1. Basic Modelling Issues, *Engineering Fracture Mechanics* 33:2 (1989) 237–252.
23. *Ibid*, 253–272.
24. R.C. McClung and H. Sehitoglu, Closure and Growth of Fatigue Cracks at Notches, ASME JEMT 114 (1992) 1–7.
25. N. Fleck, Finite Element Analysis of Plasticity Induced Crack Closure under Plane Strain Conditions, *Engineering Fracture Mechanics* 25 (1986) 441–449.
26. J. Llorca and V.S. Galvez, Modelling Plasticity-Induced Fatigue Crack Closure, *Engineering Fracture Mechanics* 37:1 (1990) 185–196.
27. M. Nakagaki and S.N. Atluri, Fatigue Crack Closure and Delay Effects Under Mode I Spectrum Loading: An Efficient Elastic-Plastic Analysis Procedure, *Fatigue of Engineering Materials and Structures* 1 (1979) 421–429.
28. J.C. Newman, Jr., A Finite-Element Analysis of Fatigue Crack Closure, in *Mechanics of Crack Growth, ASTM STP 590* (1976) 281–301.
29. M. Shiratori, T. Miyoshi, H. Miyamoto and T. Mori, A Computer Simulation of Fatigue Crack Propagation Based on the Crack Closure Concept, *Advances in Research on the Strength and Fracture of Materials*, Fourth International Conference on Fracture, Waterloo, Canada, 2B, June (1977) 1091–1098.
30. H. Sehitoglu and W. Sun, Residual Stress Fields During Fatigue Crack Growth, *Fatigue and Fracture of Engineering Materials and Structures* 15:2 (1992), 115–128.
31. B. Budiansky and J. Hutchinson, Analysis of Closure in Fatigue Crack Growth, *Journal of Applied Mechanics, Transaction of ASME* 45 (1978) 267–276.
32. J.C. Newman, Jr. and H. Armen, Jr., Elastic-Plastic Analysis of Propagating Crack Under Cyclic Loading, *AIAA Journal* 13:8 (1975) 1017–1023.
33. N. Fleck and J.C. Newman, Analysis of Crack Closure under Plane Strain Conditions, *ASTM STP 982* (1988) 319–341.
34. R.O. Ritchie, W.Yu, A.F. Blom and D.K. Holm, Response to a Discussion by A.J. McEvily, *Fatigue and Fracture of Engineering Materials and Structures* 12:1 (1989) 73–75.
35. H. Sehitoglu and W. Sun, Mechanisms of Crack Closure in Plane Strain and Plane Stress, *Fatigue under Biaxial/Multiaxial, ESIS10*, K. Kussmaul (ed.), Mechanical Engineering Publications, London (1991).
36. R.C. McClung, Crack Closure and Plastic Zone Sizes In Fatigue, *Fatigue and Fracture of Engineering Materials and Structures* 14 (1991) 455–468.
37. T.C. Lindley and C.E. Richards, The Relevance of Crack Closure to Fatigue Crack Propagation, *Materials Science and Engineering* 14 (1974) 281–293.
38. A.J. McEvily, Discussion, *Fatigue and Fracture of Engineering Materials and Structures* 12:1, (1989) 71–72.
39. N.A. Fleck and R.A. Smith, Crack Closure – Is It Just a Surface Phenomenon, *International Journal of Fatigue* 4 (1982) 157–160.
40. H.R. Shercliff and N.A. Fleck, Effect of Specimen Geometry on Fatigue Crack Growth in Plane Strain — I. Constant Amplitude Response, II. Overload Response, *Fatigue and Fracture of Engineering Materials and Structures* 13:3 (1996) 287–310.
41. H. Sehitoglu and W. Sun, Modelling of Plane Strain Fatigue Crack Closure, ASME *Journal of Engineering Materials and Technology* 113 (1990) 31–40.

42. K. Gall, H. Sehitoglu and Y. Kadioglu, F.E.M. Study of Fatigue Crack Closure Under Double Slip, *Metallurgica* (1995) to be published.
43. H. Sehitoglu, K. Gall and Y. Kadioglu, Microstructure Effects on Crack Closure, ASTM Workshop on Advances in Fatigue Crack Closure (1995).
44. K. Gall, Huseyin Sehitoglu and Yavuz Kadioglu, Plastic Zones and Fatigue Crack Closure Under Plane Strain Double Slip, *Metallurgical Transactions*, to be published.
45. A. Garcia and H. Sehitoglu, A Model for Roughness induced Crack Closure, to be submitted (1995).
46. W.L. Morris and M.R. James, Statistical Aspects of Fatigue Failure Due to Alloy Microstructure in *ASTM STP 811* (1983) 179–206.
47. P. Neumann, Coarse Slip Model of Fatigue, *Acta Metallurgica* 17 (1969) 1219.
48. R.C. McClung and H. Sehitoglu, Constraint Effects in Fatigue Crack Growth, *Proceedings 3rd International Conference on Fatigue and Fatigue Thresholds*, Charlottesville, Va. 3 (1987) 1401–1410.
49. R.C. McClung, Closure and Growth of Mode I Cracks in Biaxial Fatigue, *Fatigue and Fracture of Engineering Materials and Structures* 12:5 (1989) 447–460.
50. H. Sehitoglu and W. Wei, The Significance of Crack Closure Under High Temperature Fatigue Crack Growth with Hold Periods, *Engineering Fracture Mechanics* 33:3 (1989) 371–388.
51. K. Tanaka and Y. Nakai, Propagation and Non-Propagation of Short Fatigue Cracks at a Sharp Notch, *Fatigue of Engineering Materials and Structures* 6:4 (1983) 315–327.
52. S. Usami, Short Crack Fatigue Properties and Component Life Estimation, *Current Research on Fatigue Cracks*, MRS Vol. 1, Society of Materials Science, Japan (1985).
53. C.S. Shin and R.A. Smith, Fatigue Crack Growth from Sharp Notches, *International Journal of Fatigue* 7:2 (1985) 87–93.
54. C.S. Shin and R.A. Smith, Fatigue Crack Growth at Stress Concentrations – The Role of Notch Plasticity and Crack Closure, *Engineering Fracture Mechanics* 29:3 (1988) 301–315.
55. H. Sehitoglu, Characterization of Crack Closure, *Fracture Mechanics: Sixteenth Symposium, ASTM STP 868* (1985) 361–380.
56. S. Suresh and R.O. Ritchie, Propagation of Short Fatigue Cracks, *International Metals Reviews* 29:6 (1984) 445–476.
57. H. Sehitoglu, Crack Opening and Closure in Fatigue, *Engineering Fracture Mechanics* 21:2 (1985) 329–339.
58. B.N. Leis and T.P. Forte, Fatigue Growth of Initially Physically Short Cracks in Notched Aluminum and Steel Plates, *Fracture Mechanics: Thirteenth Conference, ASTM STP 743* (1981) 100–124.
59. K. Tanaka and Y. Nakai, Propagation and Non-Propagation of Short Fatigue Cracks at a Sharp Notch, *Fatigue of Engineering Materials and Structures* 6:4 (1983) 315–327.
60. M.M. Hammouda and K.J. Miller, Elastic Plastic Fracture Mechanics Analysis of Notches, *Elastic-Plastic Fracture, ASTM STP 668* (1979) 703–719.
61. M.M. Hammouda, R.A. Smith and K.J. Miller, Elastic-Plastic Fracture Mechanics for Initiation and Propagation of Notch Fatigue Cracks, *Fatigue of Engineering Materials and Structure* 2 (1979) 139–154.
62. S. Usami, Short Crack Fatigue Properties and Component Life Estimation, *Current Research on Fatigue Cracks*, MRS Vol. 1, Society of Materials Science, Japan (1985).
63. C.S. Shin and R.A. Smith, Fatigue Crack Growth from Sharp Notches, *International Journal of Fatigue* 7:2 (1985) 87–93.
64. C.S. Shin and R.A. Smith, Fatigue Crack Growth at Stress Concentrations – The Role of Notch Plasticity and Crack Closure, *Engineering Fracture Mechanics* 29:3 (1988) 301–315.
65. H. Sehitoglu, Fatigue Life Prediction of Notched Members Based on Local Strain and Elastic-Plastic Fracture Mechanics Concepts, *Engineering Fracture Mechanics* 18:3 (1983) 609–621.
66. R.C. McClung and H. Sehitoglu, Characterization of Fatigue Crack Growth in Intermediate and Large Scale Yielding, JEMT 113 (1991) 15–22.
67. R.C. McClung, Finite Element Modeling of Fatigue Crack Growth, International Conference on Theoretical Concepts and Numerical Analysis of Fatigue, UK (1992).
68. H.L. Ewalds and R.T. Furnee, Crack Closure Measurement Along the Fatigue Crack Front of Center Cracked Specimens, *International Journal of Fracture* 14 (1978) R53–R55.
69. D.S. Mahulikar, W.P. Slagle and H.L. Marcus, Edge Effects on Fatigue Crack Closure of Aluminum Alloys, *Scripta Matallurgica* 13 (1979) 867–880.
70. T.C. Lindley and C.E. Richards, The Relevance of Crack Closure to Fatigue Crack Propagation, *Materials Science and Engineering* 14 (1974) 281–293.
71. W.J. Mills and R.W. Hertzberg, The Effect of Sheet Thickness on Fatigue Crack Retardation in 2024-T3 Aluminum Alloy, *Engineering Fracture Mechanics* 7 (1975) 705–711.
72. K. Minakawa, G. Levan and A.J. McEvily, The Influence of Load Ration on Fatigue Crack Growth in 7090-T6 and IN9021-T4 P/M Aluminum Alloys, *Metallurgical Transactions A*, 17A (October 1986) 1787–1795.
73. A.J. McEvily, Discussion, *Fatigue and Fracture of Engineering Materials and Structures* 12:1 (1989) 71–72.

74. H. Sehitoglu, Unpublished research.
75. R.J. Asaro, Micromechanics of Crystals and Polycrystals, *Advances in Applied Mechanics*, John W. Hutchinson (ed.) 23 (1983) 1–115.
76. J.R. Rice, D.E. Hawk and R.J. Asaro, Crack Tip Fields in Ductile Crystals, *International Journal of Fracture* 42 (1990) 301–321.
77. W.T. Koiter, Stress-strain relations, uniqueness and variational theorems for elastic plastic materials with a singular yield surface. *Quarterly of Applied Mathematics* 11 (1953) 350.
78. A.J. McEvily and R.C. Boettner, On Fatigue Crack Propagation in F.C.C. Metals, *Acta Metallurgica* 11 (1963) 725–742.
79. R.M.N. Pelloux, Mechanisms of Formation of Ductile Fatigue Striations, *Transactions of the ASME* 62 (1969) 281–285.
80. N.J.I. Adams, Fatigue Crack Closure at Positive Stresses, *Engineering Fracture Mechanics* 4 (1972) 543–554.
81. V.W. Trebules, R. Roberts, Jr. and R.W. Hertzberg, ASTM STP 536 (1973) 115.
82. R.W. Hertzberg and W.J. Mills, *ASTM STP 600* (1976) 220.
83. G.T. Gray III, J.C. Williams and A.W. Thompson, Roughness-Induced Crack Closure: An Explanation for Microstructurally Sensitive Fatigue Crack Growth, *Metallurgical Transactions* 14A (1983) 421–433.
84. S.J. Balsone, J.M. Larsen, D.C. Maxwell and W.J. Jones, Effects of Microstructure and Temperature on Fatigue Crack Growth in the TiAl Alloy Ti-46.5Al-3Nb-2Cr-0.2W, *Materials Science and Engineering* A 192/193 (1995) 457–464.
85. J. Llorca, Roughness Induced Fatigue Crack Closure: A Numerical Study, *Fatigue and Fracture of Engineering Materials and Structures* 15:7 (1992) 655–669.
86. S. Suresh, Fatigue Crack Deflection and Fracture Surface Contact: Micromechanical Models, *Metallurgical Transactions* 15A (1984) 249–260.
87. K.S. Ravichandran, Fatigue Crack Growth Behavior of Small and Long Cracks in Titanium Alloys and Intermetallics, WL-TR-94-4030 (1994).
88. J.A. Greenwood and J.B.P. Williamson, Contact of Nominally Flat Surfaces, *Proceedings Royal Society London* A295 (1966) 300–19.
89. K.L. Johnson, *Contact Mechanics*, Cambridge University Press, Cambridge, UK (1985).
90. K.L. Johnson and H.R. Shercliff, Shakedown of 2-Dimensional Asperities in Sliding Contact, *International Journal of Mechanical Science* 34:5 (1992) 375–394.
91. A. Kapoor and K.L. Johnson, Steady State Topography of Surfaces in Repeated Boundary Lubricated Sliding, *Thin Films in Tribology, Leeds-Lyon Symposium on Tribology* (1993) 81–90.
92. J.A. Vazquez, A. Morrone and H. Ernst, Experimental Results on Fatigue Crack Closure for Two Aluminum Alloys, *Engineering Fracture Mechanics* 12 (1979) 231–140.
93. J.A. Vazquez, A. Morrone and J.C. Gasco, A comparative Experimental Study on the Fatigue Crack Closure Behavior Under Cyclic Loading for Steels and Aluminum Alloys, *Fracture Mechanics*, ASTM STP 677 (1979) 187–197.
94. R.C. McClung, The Influence of Applied Stress, Crack Length, and Stress Intensity Factor on Crack Closure, *Metallurgical Transactions* 22A (1991) 1559–1571.
95. H.U. Staal and J.D. Elen, Crack Closure and Influence of Cycle Ratio R on Fatigue Crack Growth in Type 304 Stainless Steel at Room Temperature, *Engineering Fracture Mechanics* 11 (1979) 275–283.
96. M.W. Brown and K.J. Miller, Mode I Fatigue Crack Growth under Biaxial Stress at Room and Elevated Temperature, *Multiaxial Fatigue, ASTM STP 853* (1985) 135–152.